HHS Public Access

Author manuscript

Mol Cancer Ther. Author manuscript; available in PMC 2018 December 01.

Published in final edited form as:

Mol Cancer Ther. 2018 June ; 17(6): 1196–1206. doi:10.1158/1535-7163.MCT-17-0682.

Nano-engineered mesenchymal stem cells increase therapeutic efficacy of anticancer drug through true active tumor targeting

Buddhadev Layek[1,‡], **Tanmoy Sadhukha**[2,3,‡], **Jayanth Panyam**[3], and **Swayam Prabha**[1,3,*]

[1]Department of Experimental and Clinical Pharmacology, College of Pharmacy, University of Minnesota, 308 Harvard Street SE, Minneapolis, MN 55455, USA

[2]Albany Molecular Research Inc., 21 Corporate Circle, Albany, NY 12203, USA

[3]Department of Pharmaceutics, College of Pharmacy, University of Minnesota, 308 Harvard Street SE, Minneapolis, MN 55455, USA

Abstract

Tumor-targeted drug delivery has the potential to improve therapeutic efficacy and mitigate non-specific toxicity of anticancer drugs. However, current drug delivery approaches rely on inefficient passive accumulation of the drug carrier in the tumor. We have developed a unique, truly active tumor targeting strategy that relies on engineering mesenchymal stem cells (MSCs) with drug-loaded nanoparticles. Our studies using the A549 orthotopic lung tumor model show that nano-engineered MSCs carrying the anticancer drug paclitaxel (PTX) home to tumors and create cellular drug depots that release the drug payload over several days. Despite significantly lower doses of PTX, nano-engineered MSCs resulted in significant inhibition of tumor growth and superior survival. Anticancer efficacy of nano-engineered MSCs was confirmed in immunocompetent C57BL/6 albino female mice bearing orthotopic Lewis Lung Carcinoma (LL/2-luc) tumors. Further, at doses that resulted in equivalent therapeutic efficacy, nano-engineered MSCs had no effect on white blood cell count whereas PTX solution and PTX nanoparticle treatments caused leukopenia. Biodistribution studies showed that nano–engineered MSCs resulted in greater than 9–fold higher AUC_{lung} of PTX (1.5 μg.day/g) than PTX solution and nanoparticles (0.2 and 0.1 μg.day/g tissue, respectively) in the target lung tumors. Furthermore, the lung-to-liver and the lung-to-spleen ratios of PTX were several folds higher for nano-engineered MSCs relative to those for PTX solution and nanoparticle groups, suggesting that nano–engineered MSCs demonstrate significantly less off-target deposition. In summary, our results demonstrate that nano-engineered MSCs can serve as an efficient carrier for tumor specific drug delivery and significantly improved anti–cancer efficacy of conventional chemotherapeutic drugs.

Keywords

Nanoparticles; mesenchymal stem cells; targeted drug delivery; lung tumor; active targeting; chemotherapy

[*]**Corresponding Author:** Tel.: +1-612-626-3545. Fax: +1-612-626-2125. prabh025@umn.edu.
[‡]Both authors contributed equally

Conflict of Interest Statement: The authors declare no potential conflicts of interest.

Introduction

Site-directed delivery of chemotherapeutic agents can improve their therapeutic index by reducing their exposure to non-target tissues. Current approaches to targeted drug delivery rely primarily on nano drug carriers that accumulate in solid tumors because of the leaky tumor vasculature. However, such passive accumulation is highly inefficient and typically less than 5% of injected dose is delivered to the tumor (1). In addition, solid tumors are characterized by elevated interstitial fluid pressure and high solid stress, both of which contribute to poor intra–tumoral distribution of the drug carriers (2).

Recent studies have investigated cell-based targeting approaches using macrophages (3), red blood cells (4), neural stem cells (5), mesenchymal stem cells (MSCs) (6) and T cells (7). Of these cell–based strategies, stem cells (8,9) and macrophages (10,11) have the potential to infiltrate specific tumor types. Concerns have been raised regarding the safety of macrophages because of their tendency to change into a tumor-promoting phenotype in response to environmental factors (12). Our studies are focused on investigating MSCs as cellular drug carriers. MSCs have been indicated for tumor-targeted therapy owing to their ability to selectively and actively home to tumors (13,14). MSCs genetically engineered to express suicide genes (cytosine deaminase, thymidine kinase, and carboxylesterase) have been shown to elicit significant antitumor response against brain tumors, ovarian, hepatocellular, pancreatic, renal or medullary thyroid carcinomas, breast and prostate cancer, and pulmonary metastases (15–17). Thus, the tumor–tropic nature of MSCs enables the possibility of true active targeting of anticancer agents to the tumor tissue. In addition, recent studies show that MSCs infiltrate tumor tissue uniformly and improve the intra–tumoral distribution of the therapeutic agent payload (18).

Previous studies with MSCs have typically involved genetic modifications to express peptides and proteins with anti–tumor properties (13,15–17). Our work is focused on non–genetic modification of MSCs by incorporating nanoparticles loaded with chemotherapeutics to create cellular drug depots capable of homing to tumors and releasing the drug over a prolonged period of time. Our previous studies show that nano–engineering of MSCs does not alter their tumor homing potential (14,19). In the current study, we investigated the anticancer effectiveness of nano–engineered MSCs carrying paclitaxel (PTX) in orthotopic models of lung cancer and the underlying mechanisms of action.

Materials and Methods

Materials

Ammonium acetate, chloroform, gentamycin, PTX, and polyvinyl alcohol (PVA) were purchased from Sigma (St. Louis, MO, USA). Fetal bovine serum and penicillin/streptomycin were obtained from Bioexpress (Kaysville, UT, USA). Dulbecco's phosphate buffered saline (DPBS), RPMI 1640 medium, and trypsin-EDTA solution were purchased from Invitrogen Corporation (Carlsbad, CA, USA). Ester-terminated 50:50 poly(DL-lactide–co-glycolide) (inherent viscosity: 0.55 – 0.75 dL/g) was procured from Lactel Absorbable Polymers (Birmingham, AL, USA). Methanol and acetonitrile was purchased from Fisher Scientific (Pittsburgh, PA, USA). Near-infrared dye SDB 5491 was acquired from HW

Sands (Jupiter, FL, USA). FITC anti-human STRO-1, Brilliant Violet 421™ anti-human CD90 (Thy1), and PE anti-human CD34 antibodies were purchased from BioLegend Antibodies (San Diego, CA, USA).

Preparation and characterization of PTX-loaded poly(lactide–co–glycolide) (PLGA) nanoparticles

PTX and an infrared dye (SDB 5491) loaded PLGA nanoparticles were formulated by emulsion-solvent evaporation technique (14). The organic phase comprised of 7 mg of PTX, 50 μg of SDB 5491 dye, and 32 mg of PLGA dissolved in 1 mL of chloroform. This mixture was emulsified in 7.5 mL of 2.5% w/v PVA using a probe sonicator (Model W-375, Heat Systems Ultrasonics Inc., Farmingdale, NY, USA) at 20 W power for 5 min. Chloroform was removed by stirring the emulsion overnight under ambient conditions, followed by one hour stirring under vacuum. The resulting nanoparticles were collected by ultracentrifugation at 35,000 rpm for 35 min at 4°C (Optima XPN-80 Ultracentrifuge, Rotor type: 50.2 Ti, Beckman Coulter, Brea, CA, USA) and washed three times with deionized water. The nanoparticle pellet was then dispersed in deionized water and centrifuged at 1000 ×g for 6 min and finally the supernatant was lyophilized (Labconco, FreeZone 4.5, Kansas City, MO, USA). Control nanoparticles containing the near-infrared dye but no PTX were formulated similarly.

The hydrodynamic diameter of nanoparticles was measured by photon correlation spectroscopy. Nanoparticles were dispersed in deionized water (0.1 mg/mL) with sonication and subjected to particle size analysis using a Delsa™ Nano C Particle Analyzer (Beckman, Brea, CA, USA) operating at a 165° constant scattering angle. To determine PTX loading, nanoparticles were dispersed in methanol (1 mg/mL) and extracted overnight using a rotary extractor. The nanoparticle dispersion was centrifuged at 13,000 rpm for 30 min (Allegra X-30R Centrifuge, Rotor type: FX 301.5, Beckman Coulter, Brea, CA, USA). The methanolic extract was used for quantification of PTX using reversed phase high-performance liquid chromatography (HPLC) (20).

Cell culture

Human mesenchymal stem cells (MSCs) isolated from human bone marrow were purchased from ScienCell Research Laboratories (Carlsbad, CA, USA) and were cultured in human mesenchymal stem cell media (ScienCell Research Laboratories). C57BL/6 mouse mesenchymal stem cells with GFP were purchased from Cyagen Biosciences, Inc. (Santa Clara, CA, USA) and were propagated in mouse mesenchymal stem cell growth medium (Cyagen Biosciences, Inc.). A549-luc-C8 (A549-luc) is a luciferase expressing cell line derived from human lung carcinoma cells, which are stably transfected with Firefly Luciferase gene, was purchased from Caliper Lifesciences (Hopkinton, MA, USA). A549-luc cells were grown in RPMI 1640 medium supplemented with 10% v/v fetal bovine serum (FBS) and 1% penicillin–streptomycin antibiotic solution. The LL/2-Red-FLuc Bioware® Brite Cell Line (LL/2-luc), a red-shifted firefly luciferase expressing cell line derived from mouse Lewis lung carcinoma, was purchased from PerkinElmer Health Sciences (Shelton, CT, USA). LL/2-luc cells were cultured in Dulbecco’s modified Eagle’s medium (DMEM) supplemented with 10% v/v FBS and 1% v/v penicillin and streptomycin. All cell lines were

maintained in a humidified incubator with 5% carbon dioxide at 37°C. All the cells were continuously monitored for morphology and growth characteristics and were used as received without any further testing. Cells were thawed and passaged 2–3 times before being used for *in vivo* or *in vitro* experimentation.

Preparation of nano-engineered MSCs

Human MSCs were used in all the studies except in the LL/2 efficacy study where both human and mouse MSCs were used. The protocol used for nanoengineering of MSCs was optimized in our previous studies (21). MSCs (2.5×10^5 cells/mL) were suspended in culture media and incubated with nanoparticles (100 μg/mL) for 4 h at 37 °C with occasional stirring. This results in the internalization of nanoparticles by MSCs through endocytosis. After 4 h of incubation, the cell suspension was centrifuged at 1,000 rpm for 5 min (Allegra X-30R Centrifuge, Rotor type: SX4400, Beckman Coulter, Brea, CA, USA) to remove un-endocytosed nanoparticles. This centrifugation step was repeated twice, with reconstitution using DPBS and the final cell pellet was resuspended in culture media for further studies.

In vitro migration potential of nano-engineered MSCs

The migration potential of nano-engineered MSCs was evaluated using a 96-Transwell® plate with 8.0 μm pores size PET membrane insert (Corning Life Sciences, Lowell, MA, USA). MSCs were serum-starved for 24 h and nano-engineered as described previously under serum-free condition. Cells were seeded in the top well at a density of 5×10^3 cells/well in 50 μL serum-free medium. The bottom well was filled with 200 μL of culture media containing 5% (v/v) serum, serum-free media or tumor conditioned media prepared by conditioning A549 lung adenocarcinoma cells for 72 h. Cells were incubated for 20 h at 37 °C in a 5% carbon dioxide incubator. After incubation, both the wells were washed with DPBS and 200 μL of Calcein AM (1.2 μg/mL) in cell dissociation solution was added to the bottom well. Following 1 h incubation in dark at 37°C, the cells suspensions were transferred to a black-walled 96-well plate and fluorescence intensities were recorded at 485/520 nm (excitation/emission) using a FLx800 microplate fluorescence reader (Biotek Inc., Winooski, VT, USA). The number of migrated nano-engineered MSCs were determined from a standard curve made with nano-engineered MSCs. Unmodified MSCs treated under similar conditions were served as positive control for this experiment.

Orthotopic lung tumor models

All animal studies were conducted in accordance with and approved by an Institutional Animal Care and Use Committee (IACUC) at the University of Minnesota. Female Fox Chase SCID® Beige mice (CB17.Cg-PrkdcscidLystbg-J/Crl) and C57BL/6 albino female mice of 6–8 weeks old were purchased from Charles River Laboratories (Wilmington, MA, USA). Orthotopic model of human lung cancer was developed in SCID® Beige mice through tail vein injection of A549-luc cells (1×10^6 cells in 200 μL of DPBS). Similarly, syngeneic mouse lung orthotopic tumors were established in immunocompetent C57BL/6 mice through tail vein injection of murine LL/2-luc cells (1×10^6 cells in 200 μL of DPBS). To monitor tumor growth, mice were injected intraperitoneally with 150 mg/kg of D-luciferin potassium salt solution (Gold Biotechnology, St. Louis, MO, USA) and tumor

associated bioluminescence was recorded using an IVIS Spectrum In Vivo Imaging System (Caliper Life Sciences, Hopkinton, MA, USA).

Anticancer efficacy of nano-engineered MSCs in orthotopic lung tumor models

SCID® Beige mice with A549-luc tumor bioluminescence of 10^5–10^6 photons/sec were randomly divided into six groups receiving intravenous injection of saline, untreated MSCs (1×10^6 on day 0 and 0.5×10^6 MSCs at every 14 days; MSC), MSCs incubated with blank (drug free) nanoparticles (1×10^6 on day 0 and 0.5×10^6 MSCs at every 14 days; MSC + Blank NP), PTX solution (administered at 40 mg/kg on day 0, 4, and 8; PTX solution), PTX loaded nanoparticles (administered at 40 mg/kg on day 0, 4, and 8; PTX NP), and MSCs preincubated with PTX loaded nanoparticles (1×10^6 on day 0 and 0.5×10^6 MSCs at every 14 days; MSC+PTX NP). PTX solution and nanoparticle formulation dosing regimen was selected based on other pre-clinical studies that demonstrate that this dosing regimen is effective in inhibiting lung tumor growth (22). Anticancer efficacy of nano-engineered MSCs was further evaluated in C57BL/6 mice bearing orthotopic LL/2-luc tumors. Mice that developed tumors were divided into nine groups receiving intravenous injection of saline, untreated MSCs, MSC + Blank NP, PTX solution, PTX NP, and MSC + PTX NP as described for A549-luc tumor model. In this study, mice treated with MSC, MSC + Blank NP, and MSC + PTX NP received a second full dose of MSCs on day 14 (instead of half the dose as was done in the A549-luc tumor model). Additional groups included untreated mouse MSCs (3×10^6 MSCs on day 0 and 14; mMSC), mouse MSCs incubated with blank nanoparticles (3×10^6 MSCs on day 0 and 14; mMSC + Blank NP), and mouse MSCs preincubated with PTX loaded nanoparticles (3×10^6 MSCs on day 0 and 14; mMSC + PTX NP). The dose of mouse MSCs was selected based on the equivalent PTX loading. Animals were imaged at predetermined time points to monitor lung bioluminescence. Mice were euthanized when they showed signs of stress such as loss of appetite, weight loss, and ruffled hair. The lung tumors were collected at the end of the study and saved at −80 °C for further analysis.

Safety of nano-engineered MSCs

Hematologic and liver toxicity profile was evaluated in tumor free C57BL/6 mice following administration of the different treatments that were used in the efficacy studies. Mice were randomly divided into five groups (8 animals in each group) and were administered intravenous injection of saline, MSC + Blank NP (1×10^6 cells on day 0), PTX solution (administered at 40 mg/kg on day 0 and 4), PTX NP (administered at 40 mg/kg on day 0 and 4), and MSC + PTX NP (1×10^6 cells on day 0). For complete blood count (CBC), blood (about 250 μL per mouse) was collected from four mice of each group into EDTA tubes and gently mixed to prevent sample clotting. For liver function test, blood (about 200 μL per mouse) was collected from remaining four mice of each group into heparin-coated tube and pooled together. Blood samples were analyzed at Charles River Clinical Pathology Services (Shrewsbury, MA, USA).

Biodistribution of nano-engineered MSCs

Biodistribution profile of nano-engineered MSCs was determined in A549-luc orthotopic lung tumor model. For efficient tracking and quantification, MSCs were nano-engineered

with SDB 5491 dye loaded nanoparticles. Mice having a lung tumor bioluminescence of 10^5–10^6 photons/sec were injected intravenously with 2.5×10^5 nano-engineered MSCs via tail vein (n = 5 per group) and the resulting fluorescence profiles were imaged at 10 min, 1 h, 4 h, 1 d, 2 d, 4 d, 6 d, and 8 d post injection. The distribution of the nano-engineered MSCs was observed based on the intrinsic fluorescence of SDB 5491 dye (λ_{ex}: 745 and λ_{em}: 820 nm). The fluorescence images were captured and analyzed using Living Image® software version 4.2 (Caliper Life Sciences, Hopkinton, MA, USA).

Immunohistological staining of nano-engineered MSCs *in vivo*

Untreated MSCs, nano-engineered MSCs, and A549-luc cells were seeded in 8-chamber slides (Nunc™ Lab-Tek™ II Chamber Slide™ System, Rochester, NY, USA) at a density of 5×10^3 cells/well and incubated overnight at 37°C and 5% carbon dioxide. Following DPBS washes, cells were fixed in ice-cold methanol for 5 min and blocked with 1% (w/v) bovine serum albumin for 1.5 h at room temperature. Cells were then incubated with Brilliant Violet 421™ anti-human CD90 (Thy1), FITC anti-human STRO-1, and PE anti-human CD34 antibodies for 1 h at room temperature. After washing with DPBS three times, cells were mounted with coverslip using SlowFade® gold antifade mount (Molecular Probes, Inc., Eugene, OR, USA) mounting medium. The stained cells were photographed with an Olympus FluoView FV1000 BX2 upright confocal microscope (Olympus Corporation, Tokyo, Japan) using a 20×/1.30 numerical aperture oil-immersion objective. The images were captured and analyzed using FV1000 Viewer software (FV 1000-ASW ver. 2.1c, Olympus Corporation, Tokyo, Japan) and ImageJ software (NIH), respectively.

In vivo distribution of PTX

The tumor-bearing animals were distributed randomly into 3 groups receiving 5 μg PTX per mouse in the form of 10 mg/mL DMSO solution diluted in DPBS, PTX and infrared dye loaded nanoparticles, and nano-engineered MSCs. After intravenous injection of the treatments, the three animals from each group were euthanized at 2 h, 1 d, 2 d, 5 d, and 12 d by carbon dioxide euthanasia and blood, liver, spleen, and lungs were collected. Blood samples were collected by cardiac puncture into Capiject® tubes and centrifuged at 13,500 rpm for 10 minutes to separate the plasma from the cells. Plasma and other tissue samples were stored at −80°C until processed for LC-MS/MS analysis. Additionally, one set of animals received a second dose of the initial treatment at 12 d. Those animals were euthanized 2 h after redosing and blood and other organs were collected as described earlier. Tissues from untreated tumor-bearing mice were used as blank controls.

Tissue samples were homogenized in DPBS (1 mL for lungs and spleen, and 2 mL for liver) using a PowerGen 125 tissue homogenizer (Fisher Scientific, Waltham, MA, USA). The tissue homogenate was spiked with 50 μL of 1.5 μg/mL docetaxel (internal standard, IS) and extracted using 5 mL of tertiary butyl methyl ether (TBME). Plasma and tissues from controlled mice were spiked with PTX to determine its extraction efficiency. The mixture was vortexed for 5 min, followed by centrifugation for 20 min at 4,000 rpm (Centrifuge 5810 R, Eppendorf AG, Hamburg, Germany). The organic layer (4 mL) was transferred into a new tube and evaporated at room temperature under nitrogen flow (N-EVAP™, Organomation, Berlin, MA, USA). The residue was reconstituted in 150 μL of methanol and

used for LC-MS/MS analysis. For plasma, 100 μL of sample was spiked with 50 μL of internal standard and extracted with 1.2 mL of TBME. The mixture was then vortexed and centrifuged like other tissue samples. One milliliter of the ether extract was dried and reconstituted in 150 μL methanol for LC-MS/MS analysis.

The concentrations of PTX was determined by Aquity UPLC® System (Waters, Milford, MA, USA) coupled with Waters/Micromass Quattro Ultima LC/MS/MS mass spectrometer (Waters, Milford, MA, USA). Separation of PTX and IS was performed on the Zorbax Eclipse XDB-C18 (50 mm ×4.6 mm, 1.8 μm) analytical column (Agilent Technologies, CA, USA). Five microliter of the processed sample was injected into the column using a temperature-controlled auto sampler maintained at 10°C. The isocratic mobile phase composed of a mixture of methanol and 0.1% (v/v) formic acid in water (75:25, v/v) at a flow rate of 0.4 mL/min. Mass spectrometric detection of PTX and IS was carried out in positive ion mode using a triple quadrupole mass spectrometer (Waters, Milford, MA, USA), equipped with an electrospray ionization interface operating at a capillary voltage of 3 kV and cone voltage of 50 V. The collision energy was set at 33 V for PTX and 30 V for IS. Detection of the ions was performed in multiple-reaction monitoring mode, monitoring the transition ion pair m/z 876.22/307.91 for PTX and m/z 830.16/548.97 for the IS. The dwell time per transition was 0.4 sec for both PTX and IS. Data acquisition and peak integration were achieved by MassLynx software, version 4.1. The assay was sensitive and linear over a range of 1 ng/mL to 1,000 ng/mL. Pharmacokinetic parameters in blood, lungs, liver, and spleen were determined using Phoenix WinNonlin 6.4 software (Pharsight Corporation, Mountain View, CA).

Immunohistological analysis of tumors

The tumors were fixed in 4% (w/v) formaldehyde solution for 24 h followed by storage in 70% ethanol. The fixed tumors were processed, paraffin-embedded, and cut at 4 μm thick slices. The sections were stained for cleaved caspase-3 (for apoptosis), Ki-67 (for tumor proliferation), and CD31 (for angiogenesis). Both cleaved-caspase 3 (Cell Signaling Technology, Danvers, MA, USA) and Ki-67 clone SP-6 (Biocare, Concord, CA, USA) utilized a 1:100 antibody concentration followed by Envision Rabbit Horseradish Peroxidase (HRP) detection system (Dako, Carpenteria, CA, USA). CD31assay utilized a 1:1200 antibody concentration (Santa Cruz, Dallas, TX, USA) followed by Goat-on-Rodent (HRP) polymer system (Biocare, Concord, CA, USA). All sections were developed using DAB chromogen (Dako) and counterstained with Mayer’s Hematoxylin (Dako). The relative staining for each target was analyzed by ImageJ software (Bethesda, MD, USA) to determine the fraction of positive stain per unit tissue area.

Statistical analyses

Statistical analyses were performed using one-way ANOVA, followed by Bonferroni-Holm *post-hoc* analysis for comparison between individual groups. Log-rank test was conducted to compare the survival distribution of different treatment groups. A probability level of $P < 0.05$ was considered significant.

Results

Preparation and characterization of PTX-loaded PLGA nanoparticles

PLGA nanoparticles loaded with PTX and a near-infrared fluorescent dye (SDB 5491) were fabricated with a mean hydrodynamic diameter of 282.5 ± 5.2 nm and a polydispersity index of 0.21. Nanoparticles exhibited a net negative surface charge of −18.4 ± 2.5 mV. PTX loading in nanoparticles was 18.1 ± 1.9 % (w/w).

Preparation and characterization of nano-engineered MSCs

Nano–engineered MSCs were prepared using our optimized protocol reported previously (21). The *in vitro* migratory behavior of nano–engineered MSCs was similar to that of untreated MSCs, with about 3.1–3.5–fold increase in migration towards serum or tumor–reconditioned media compared to that towards serum–free medium (Figure S1).

Anticancer efficacy of nano-engineered MSCs in orthotopic lung tumor models

Anticancer efficacy of nano-engineered MSCs was evaluated in both A549-luc human lung adenocarcinoma model and syngeneic murine LL/2-luc lung tumor model. Orthotopic lung tumors were formed by intravenous injection of A549-luc human lung adenocarcinoma cells that were stably transfected with luciferase gene (23). Treatment with nano–engineered MSCs resulted in significant inhibition of the lung tumor growth ($P < 0.0001$) compared to that with other controls (Figure 1A). The therapeutic effectiveness of nano–engineered MSCs also manifested in the superior survival rates compared to that with other controls (Figure 1B). While the animals in the control groups died between 35–98 days after treatment, the mean survival of nano–engineered MSCs treated animals was 147 days. Similar results were obtained in the syngeneic murine LL/2-luc lung tumor model (Figure 1C). Despite significantly lower doses of PTX (~2.5 mg/kg total dose for nanoengineered MSCs Vs 120 mg/kg for free- and nanoparticle-encapsulated drug), nano-engineered MSCs resulted in similar or slightly greater tumor inhibition (Figure 1C inset). We also compared the relative effectiveness of human and mouse MSCs. As shown in Figure 1D, nano-engineered mouse MSCs were also effective in inhibiting tumor growth compared to non-drug controls (Figure 1D). It was interesting to note that both nano-enginerred human and mouse MSCs had similar anticancer activity in this immuno-competent mouse tumor model.

Safety of nano-engineered MSCs

PTX is known to cause dose-dependent hematologic toxicities, particularly leukopenia and neutropenia (24,25). Similarly, PTX induced abnormalities in liver enzymes including aspartate aminotransferase, alkaline phosphatase, and bilirubin has been reported in clinical trials (26). Therefore, the effect of different treatments on hematological and biochemical parameters were evaluated. Treatments with PTX solution and PTX NP ($P < 0.05$) resulted in about 25–45% decrease in white blood cell (WBC) count, however, MSC + Blank NP and MSC + PTX NP did not alter the WBC count (Table 1 and Table S1). Moreover, PTX solution treatment resulted in significantly decreased ($P < 0.05$) red blood cell (RBC) count and hemoglobin concentration compared to saline treated mice. PTX solution and PTX NP also resulted in slightly elevated alanine aminotransferase (ALT) levels and a decrease in the

alkaline phosphatase (ALP) levels (Table 2 and Table S2). Nano-engineered MSCs did not alter any of the liver enzymes.

Biodistribution of nano-engineered MSCs

MSCs engineered with NIR dye-labeled nanoparticles were injected in both tumor– and non–tumor bearing mice. Our studies showed that nano–engineered MSCs accumulated in the lungs at early time points, irrespective of the tumor burden (Figure 2A and B). Interestingly, by 24 h, MSCs cleared from the lungs of healthy, non–tumor bearing animals. By 48 h, most of the fluorescence from thoracic area disappeared, and instead, strong fluorescence signal was detected in the abdomen. In contrast, MSC–associated fluorescence was present in the lungs with tumors even after 8 days following injection, suggesting prolonged residence of MSCs in the lungs of tumor–bearing animals. Even within tumor–bearing animals, fluorescence could be detected only in the lungs with tumor and not in the lungs without tumor (Figure 2C), suggesting that MSCs are not simply trapped in the lung vasculature.

Intra–tumoral localization of nano-engineered MSCs

To further confirm that the enhanced fluorescent signal observed in the lung tumors in the above study was because of MSC accumulation and not from free dye, we performed IHC on lung tumor tissues isolated from treated mice on day 8 after treatment initiation. Viable MSCs have previously been identified by the presence of cell surface markers such as CD90 (Thy-1), Stro–1, CD44, CD105, CD106, SSEA–4, CD271, and CD146 and the absence of CD19, CD34, and CD45 among others (27,28). In order to determine the most suitable marker to differentiate the A549-luc lung cancer cells from nano–engineered MSCs, we stained the cells with STRO–1, CD90, and CD34 antibody (28). CD34 and STRO–1 were unsuitable for detection of MSCs in our study because A549-luc cells also showed similar staining pattern as that of MSCs (Figure S2). However, MSCs stained strongly for CD90, which was absent on A549-luc cells (Figure 3A). In addition, nano–engineered MSCs (MSC + PTX NP) had a similar high CD90 staining as the unmodified MSCs (Figure 3A), confirming that CD90 could be used reliably for the identification of MSCs.

As can be seen from Figure 3B, both nano–engineered MSCs (MSC + PTX NP) and unmodified MSCs were found in and around tumor cells at 8 days post treatment. Untreated tissues did not stain for MSCs. Distinct CD90 staining on the surface of viable cells suggests that the MSCs were viable several days after localizing in the lung tumors.

In vivo biodistribution of PTX

We also evaluated whether nano-engineered MSCs resulted in enhanced tumor delivery of the drug. We analyzed the amount of PTX present in circulation, in tumor–bearing lungs, and in clearance organs such as liver and spleen at different time points after administration of PTX free in solution, encapsulated in nanoparticles and in the form of nano–engineered MSCs (Figure 4A). The plasma concentration of PTX after intravenous injection of the soluble drug followed a biexponential decay, characterized by a rapid distribution to the different organs followed by a slower clearance of the drug from the body. Nano-engineered MSCs maintained the PTX concentration in plasma for a much longer duration, resulting in

higher AUC of the drug in the plasma. The overall AUC_{plasma} of PTX between 2 h and 12 days was 1.3 μg.day/L for PTX solution, 3.0 μg.day/L for PTX nanoparticles and 6.0 μg.day/L for nano–engineered MSCs.

Concentration of PTX in the lungs 2 h post injection was 9–fold higher for nano–engineered MSCs compared to PTX solution (Figure 4B). This elevated lung deposition of nano–engineered MSCs resulted in greater than 9–fold higher AUC_{lung} of PTX delivered as nano–engineered MSCs (1.5 μg.day/g tissue) compared to PTX solution and nanoparticles (0.2 and 0.1 μg.day/g tissue, respectively). The overall concentration of PTX in the lung was consistently about an order of magnitude higher with nano–engineered MSCs than other formulations. Furthermore, the lung concentration of PTX was much higher at 12 days with nano–engineered MSCs compared to other treatments.

Furthermore, the lung-to-liver and the lung-to-spleen ratios of PTX were several folds higher for nano-engineered MSCs relative to those for PTX solution and nanoparticle groups (Figure 4 C and D). This suggests that unlike free drug and nanoparticle treatments, nano–engineered MSCs demonstrate significantly less off-target deposition.

Effect of nano-engineered MSCs on tumor cell proliferation and induction of apoptosis

Tumor samples were stained for cleaved caspase 3, Ki-67, and CD31 to determine the effect of various treatments on induction of apoptosis, cell proliferation and angiogenesis, respectively (Figure 5A). Treatment with nano–engineered MSCs significantly reduced cell proliferation in the tumor tissue as evidenced by the lower number of Ki-67 positive cells relative to that in other treatment groups (Figure 5B). Similarly, treatment with nano–engineered MSCs significantly reduced tumor angiogenesis. Microvessel density was significantly higher in the case of saline, MSC, and MSC+Blank NP treated animals than free PTX and PTX nanoparticle treated animals. However, animals treated with nano-engineered MSCs were characterized by significantly fewer CD31 positive blood vessels ($P < 0.01$) compared to all other groups (Figure 5C). An inverse staining profile was observed for cleaved caspase 3. Treatment with nano-engineered MSCs induced significantly higher cleaved caspase-3 levels in tumor compared to all other groups (Figure 5D).

Discussion

The utility of cytotoxic drugs such as PTX in the treatment of cancer is often limited by their severe, dose-limiting toxicities. For example, myelosuppression and peripheral neuropathy are major side effects of PTX therapy. Nanoparticulate systems such as Abraxane (29) and Doxil (30) can improve the delivery of anticancer drugs to the tumor tissue while reducing the exposure to normal tissues. Such systems rely on the leaky vasculature found in solid tumors to passively accumulate in the tumor, a highly inefficient process (31). Active targeting approaches seek to target receptors or other membrane proteins that are overexpressed in tumors to enhance tumor cell specific accumulation of the drug carriers (32). However, such systems have to first passively accumulate in the tumor before they can bind with tumor cells. Thus, active or ligand-based targeting approaches have similar limitations as that of passive targeting (33).

MSCs have shown considerable promise in cancer therapy. MSCs can be isolated from various tissues including bone marrow and adipose, and can successfullly be grown in petri plates *in vitro* (34). Further, MSCs do not pose significant immunogenicity concerns owing to low or no expression of HLA class I and class II molecules (35). Absence of co-stimulatory molecules such as CD40, 80 and 86, which are responsible for initiation of immune response, lends to universal acceptance of allogeneic MSCs (36,37). MSCs that are genetically modified to express anticancer macromolecules have shown promising anticancer effectiveness in various tumor models (9,13,38). However, MSCs have not been pursued as carriers for small molecules, likely because of the difficulty in immobilizing small molecules in cells for durations required to achieve tumor targeting without affecting their viability or tumor tropism. Overexpression of drug efflux transporters such as P-glycoprotein (21,39) in these cells further limits the loading of anticancer drugs, many of which are substrates for efflux transporters (40).

We have developed a nano-engineering strategy that enables the incorporation of small molecules in MSCs (21). We used PTX as a model anticancer agent because of its effectiveness against lung cancer (41,42). Polymeric nanoparticles formulated with a biodegradable and biocompatible polymer, poly(DL-lactide-co-glycolide) (PLGA), was used to load PTX in MSCs (43). Previous studies have shown that following endocytic uptake into cells, PLGA nanoparticles escape the endo-lysosomes and are retained in the cytoplasm for several days (44). Once the drug is released intracellularly within MSCs, it can diffuse out of the cell or be effluxed out by the transporters (45). The drug is then available to kill the cancer cells.

In the current study, we evaluated the anti-cancer efficacy of nano-engineered MSCs in both orthotopic A549-luc human adenocarcinoma model and syngeneic murine LL/2-luc lung tumor model. It was interesting to note that despite the significantly lower amount of PTX used (~9 mg/kg total dose for nano-engineered MSCs Vs 120 mg/kg for PTX solution and nanoparticles), nano–engineered MSCs were significantly more effective in inhibting A549 tumor growth than PTX nanoparticles, suggesting better drug delivery to the tumor. Similarly, despite significantly lower doses of PTX, nano-engineered MSCs resulted in greater tumor inhibition in the syngeneic mouse model. However, the overall tumor growth inhibition in the A549 tumor model was higher than that observed in the LL/2 model. This could be due to the fact that LL/2 is a more aggressive tumor model than the A549 tumor model (46). Time to reach maximum tumor volumes in untreated animals was much shorter for LL2 tumors (3 weeks Vs 10 weeks for A549).

It was also interesting to note that two doses of human or mouse nano-engineered MSCs resulted in similar therapeutic effect in the immune-competent mouse tumor model, suggesting that an intact immune system does not affect the ability of MSCs to home to tumor. This is consistent with several previous studies demonstrating that MSCs do not evoke an immune response because of lack of expression of HLA class I and II molecules and costimulatory molecules such as CD40, 80, and 86, which are responsible for immune response (47).

Tumor tropism is a key requirement for using MSCs in tumor targeting. Particles larger than 6 micron (48) and cells can accumulate in lungs (49) after intravenous injection due to pulmonary first pass effect. In order to determine whether nano–engineered MSCs were passively accumulating in the lungs or were actively homing to the tumors, we evaluated the *in vivo* biodistribution and tumor targeting of nano–engineered MSCs. Our studies show that nano-engineered MSCs accumulated in the lungs in the early time points, irrespective of the tumor burden, but were cleared from the healthy lungs by 48 hours. In contrast, we saw prolonged residence of MSCs in the lungs of animals with lung tumors. In animals that had tumors in only one of the lungs, MSCs accumulated only in the lung with the tumors, confirming that MSCs are not simply trapped in the lung vasculature.

There is some debate in the literature regarding the ability of MSCs to actively traffic to tumors. MSCs possess surface markers such as SDF-1, IFN-γ, CCL5/CCR5, and CCR2 that allow them to home to sites of inflammation *in vivo* (50). Tumor microenvironment is rich in pro-inflammatory cytokines, which act as chemoattractants for MSCs (50). Kidd et al. showed that following intravenous injection in healthy mice, MSCs migrated to the lung and then to the liver and spleen (51). In mice bearing MDA-MB-231 metastatic tumors, intravenously injected MSCs demonstrated tropism for lung metastasis. In contrast, Wang et al reported a lack of tumor targeting in breast cancer xenografts following intravenous injection of MSCs (52). However, the fate of MSCs was followed only for a short period of time after IV dosing. It is possible that the duration of the study was not long enough to detect MSCs in tumors. Our studies, performed over several days, provide strong evidence for the ability of nano-engineered MSCs to actively traffic to the tumor tissue *in vivo*. Further, our studies demonstrated significantly higher accumulation of PTX in tumors compared to clearance organs such as liver and spleen in the mice injected with nano-engineered MSCs, pointing to their active trafficking to the tumor. Sustained retention of MSCs, in conjunction with slow release of the drug, likely contributes to prolonged exposure of tumor cells to the drug.

A major impediment to the success of anticancer delivery systems is non-homogenous distribution of the carrier within the tumor. High interstitial fluid pressure and solid stress exerted by the tumor extracellular matrix inhibit nanoparticle transport within tumors (53) and reduce the fraction of the drug that is able to reach cells that are more remote - often the aggressive tumor population (54). IHC studies show that nano-engineered MSCs were found in and around tumor cells, suggesting that MSCs can allow for better intra-tumoral distribution of the therapeutic agent.

PTX has been shown to inhibit tumor growth through both a direct cytostatic effect on tumor cells as well as through inhibition of angiogenesis (55). IHC studies confirmed that PTX delivered using nano-engineered MSCs resulted in decreased tumor cell proliferation, inhibited angiogenesis and increased apoptosis within the tumor matrix. These results are consistent with increased PTX delivery to the tumor and greater inhibition of tumor growth observed in our studies.

In summary, our studies show that nano-engineered MSCs actively migrate to lung tumors, where they are retained for several days, thereby facilitating targeted and sustained delivery

of the drug payload. This results in significantly improved anti–cancer efficacy at a considerably reduced dose of the drug. This dose-sparing effect of nano-engineered MSCs mitigated leukopenia, a common side effect of PTX. Thus, these studies demonstrate the true active targeting potential of nano-engineered MSCs.

Supplementary Material

Refer to Web version on PubMed Central for supplementary material.

Acknowledgments

The authors would like to thank Paula Overn (Comparative Pathology Shared Resource) for immunohistological staining of tumor tissues. Live animal imaging (bioluminescence and fluorescent imaging) was performed at the University Imaging Center at the University of Minnesota (Minneapolis, MN).

Financial Information: The work was supported by funding from NIH (EB022558; S Prabha and J. Panyam), University of Minnesota Grant in Aid program (S. Prabha) and the College of Pharmacy-College of Veterinary Medicine collaborative research grant at the University of Minnesota (S. Prabha).

References

1. Bae YH, Park K. Targeted drug delivery to tumors: myths, reality and possibility. Journal of controlled release : official journal of the Controlled Release Society. 2011; 153:198–205. [PubMed: 21663778]
2. Stylianopoulos T, Martin JD, Snuderl M, Mpekris F, Jain SR, Jain RK. Coevolution of solid stress and interstitial fluid pressure in tumors during progression: implications for vascular collapse. Cancer research. 2013; 73:3833–41. [PubMed: 23633490]
3. Choi MR, Bardhan R, Stanton-Maxey KJ, Badve S, Nakshatri H, Stantz KM, et al. Delivery of nanoparticles to brain metastases of breast cancer using a cellular Trojan horse. Cancer nanotechnology. 2012; 3:47–54. [PubMed: 23205151]
4. Chambers E, Mitragotri S. Long circulating nanoparticles via adhesion on red blood cells: mechanism and extended circulation. Experimental biology and medicine. 2007; 232:958–66. [PubMed: 17609513]
5. Cheng Y, Morshed R, Cheng SH, Tobias A, Auffinger B, Wainwright DA, et al. Nanoparticle-programmed self-destructive neural stem cells for glioblastoma targeting and therapy. Small. 2013; 9:4123–9. [PubMed: 23873826]
6. Roger M, Clavreul A, Venier-Julienne MC, Passirani C, Sindji L, Schiller P, et al. Mesenchymal stem cells as cellular vehicles for delivery of nanoparticles to brain tumors. Biomaterials. 2010; 31:8393–401. [PubMed: 20688391]
7. Huang B, Abraham WD, Zheng Y, Bustamante Lopez SC, Luo SS, Irvine DJ. Active targeting of chemotherapy to disseminated tumors using nanoparticle-carrying T cells. Science translational medicine. 2015; 7:291ra94.
8. Muller FJ, Snyder EY, Loring JF. Gene therapy: can neural stem cells deliver? Nature reviews Neuroscience. 2006; 7:75–84. [PubMed: 16371952]
9. Nakamizo A, Marini F, Amano T, Khan A, Studeny M, Gumin J, et al. Human bone marrow-derived mesenchymal stem cells in the treatment of gliomas. Cancer research. 2005; 65:3307–18. [PubMed: 15833864]
10. Batrakova EV, Li S, Reynolds AD, Mosley RL, Bronich TK, Kabanov AV, et al. A macrophage-nanozyme delivery system for Parkinson's disease. Bioconjugate chemistry. 2007; 18:1498–506. [PubMed: 17760417]
11. Zhao Y, Haney MJ, Klyachko NL, Li S, Booth SL, Higginbotham SM, et al. Polyelectrolyte complex optimization for macrophage delivery of redox enzyme nanoparticles. Nanomedicine (Lond). 2011; 6:25–42. [PubMed: 21182416]

12. Mosser DM, Edwards JP. Exploring the full spectrum of macrophage activation. Nature reviews Immunology. 2008; 8:958–69.
13. Chen X, Lin X, Zhao J, Shi W, Zhang H, Wang Y, et al. A tumor-selective biotherapy with prolonged impact on established metastases based on cytokine gene-engineered MSCs. Mol Ther. 2008; 16:749–56. [PubMed: 18362930]
14. Layek B, Sadhukha T, Prabha S. Glycoengineered mesenchymal stem cells as an enabling platform for two-step targeting of solid tumors. Biomaterials. 2016; 88:97–109. [PubMed: 26946263]
15. Kucerova L, Matuskova M, Pastorakova A, Tyciakova S, Jakubikova J, Bohovic R, et al. Cytosine deaminase expressing human mesenchymal stem cells mediated tumour regression in melanoma bearing mice. The journal of gene medicine. 2008; 10:1071–82. [PubMed: 18671316]
16. Song C, Xiang J, Tang J, Hirst DG, Zhou J, Chan KM, et al. Thymidine kinase gene modified bone marrow mesenchymal stem cells as vehicles for antitumor therapy. Human gene therapy. 2011; 22:439–49. [PubMed: 20925460]
17. Yin J, Kim JK, Moon JH, Beck S, Piao D, Jin X, et al. hMSC-mediated concurrent delivery of endostatin and carboxylesterase to mouse xenografts suppresses glioma initiation and recurrence. Mol Ther. 2011; 19:1161–9. [PubMed: 21386822]
18. Bexell D, Gunnarsson S, Svensson A, Tormin A, Henriques-Oliveira C, Siesjo P, et al. Rat multipotent mesenchymal stromal cells lack long-distance tropism to 3 different rat glioma models. Neurosurgery. 2012; 70:731–9. [PubMed: 21869725]
19. Sadhukha T, O'Brien TD, Prabha S. Nano-engineered mesenchymal stem cells as targeted therapeutic carriers. J Control Release. 2014; 196:243–51. [PubMed: 25456830]
20. Patil Y, Sadhukha T, Ma L, Panyam J. Nanoparticle-mediated simultaneous and targeted delivery of paclitaxel and tariquidar overcomes tumor drug resistance. Journal of controlled release : official journal of the Controlled Release Society. 2009; 136:21–9. [PubMed: 19331851]
21. Sadhukha T, O'Brien TD, Prabha S. Nano-engineered mesenchymal stem cells as targeted therapeutic carriers. Journal of controlled Release. 2014; 196:243–51. [PubMed: 25456830]
22. Kirtane AR, Sadhukha T, Kim H, Khanna V, Koniar B, Panyam J. Fibrinolytic Enzyme Cotherapy Improves Tumor Perfusion and Therapeutic Efficacy of Anticancer Nanomedicine. Cancer research. 2017; 77:1465–75. [PubMed: 28108516]
23. Sadhukha T, Wiedmann TS, Panyam J. Inhalable magnetic nanoparticles for targeted hyperthermia in lung cancer therapy. Biomaterials. 2013; 34:5163–71. [PubMed: 23591395]
24. Alsharedi M, Gress T, Dotson J, Elmsherghi N, Tirona MT. Comparison of toxicity profile and tolerability between two standard of care paclitaxel-based adjuvant chemotherapy regimens in breast cancer. Medical Oncology. 2016; 33:27. [PubMed: 26883934]
25. Spencer CM, Faulds D. Paclitaxel. A review of its pharmacodynamic and pharmacokinetic properties and therapeutic potential in the treatment of cancer. Drugs. 1994; 48:794–847. [PubMed: 7530632]
26. Mandaliya H, Baghi P, Prawira A, George MK. A Rare Case of Paclitaxel and/or Trastuzumab Induced Acute Hepatic Necrosis. Case Reports in Oncological Medicine. 2015; 2015:2.
27. Lv FJ, Tuan RS, Cheung KM, Leung VY. Concise review: the surface markers and identity of human mesenchymal stem cells. Stem Cells. 2014; 32:1408–19. [PubMed: 24578244]
28. Boxall SA, Jones E. Markers for characterization of bone marrow multipotential stromal cells. Stem Cells Int. 2012; 2012:975871. [PubMed: 22666272]
29. Higuchi M, Takagi H, Owada Y, Inoue T, Watanabe Y, Yamaura T, et al. Efficacy and tolerability of nanoparticle albumin-bound paclitaxel in combination with carboplatin as a late-phase chemotherapy for recurrent and advanced non-small-cell lung cancer: A multi-center study of the Fukushima lung cancer association group of surgeons. Oncol Lett. 2017; 13:4315–21. [PubMed: 28599432]
30. Barenholz Y. Doxil(R)--the first FDA-approved nano-drug: lessons learned. Journal of controlled release : official journal of the Controlled Release Society. 2012; 160:117–34. [PubMed: 22484195]
31. Davis ME, Chen ZG, Shin DM. Nanoparticle therapeutics: an emerging treatment modality for cancer. Nature reviews Drug discovery. 2008; 7:771–82. [PubMed: 18758474]

32. Torchilin VP. Passive and active drug targeting: drug delivery to tumors as an example. Handbook of experimental pharmacology. 2010:3–53.
33. Chen Weihsu C, Zhang Andrew X, Li S-D. Limitations and niches of the active targeting approach for nanoparticle drug delivery. European Journal of Nanomedicine. 42012:89.
34. Gnecchi M, Melo LG. Bone marrow-derived mesenchymal stem cells: isolation, expansion, characterization, viral transduction, and production of conditioned medium. Methods in molecular biology. 2009; 482:281–94. [PubMed: 19089363]
35. Klyushnenkova E, Mosca JD, Zernetkina V, Majumdar MK, Beggs KJ, Simonetti DW, et al. T cell responses to allogeneic human mesenchymal stem cells: immunogenicity, tolerance, and suppression. Journal of biomedical science. 2005; 12:47–57. [PubMed: 15864738]
36. Atoui R, Asenjo JF, Duong M, Chen G, Chiu RC, Shum-Tim D. Marrow stromal cells as universal donor cells for myocardial regenerative therapy: their unique immune tolerance. The Annals of thoracic surgery. 2008; 85:571–9. [PubMed: 18222266]
37. Le Blanc K, Rasmusson I, Sundberg B, Gotherstrom C, Hassan M, Uzunel M, et al. Treatment of severe acute graft-versus-host disease with third party haploidentical mesenchymal stem cells. Lancet. 2004; 363:1439–41. [PubMed: 15121408]
38. Loebinger MR, Eddaoudi A, Davies D, Janes SM. Mesenchymal stem cell delivery of TRAIL can eliminate metastatic cancer. Cancer research. 2009; 69:4134–42. [PubMed: 19435900]
39. Kim SG, Jeon CH, Suh HS, Choe JY, Shin IH. P-glycoprotein expression in extracellular matrix formation of chondrogenic differentiation of human adult stem cells. Cell biology international. 2007; 31:1042–8. [PubMed: 17468018]
40. Holohan C, Van Schaeybroeck S, Longley DB, Johnston PG. Cancer drug resistance: an evolving paradigm. Nature reviews Cancer. 2013; 13:714–26. [PubMed: 24060863]
41. Green MR, Manikhas GM, Orlov S, Afanasyev B, Makhson AM, Bhar P, et al. Abraxane, a novel Cremophor-free, albumin-bound particle form of paclitaxel for the treatment of advanced non-small-cell lung cancer. Ann Oncol. 2006; 17:1263–8. [PubMed: 16740598]
42. Hu J, Fu S, Peng Q, Han Y, Xie J, Zan N, et al. Paclitaxel-loaded polymeric nanoparticles combined with chronomodulated chemotherapy on lung cancer: In vitro and in vivo evaluation. Int J Pharm. 2017; 516:313–22. [PubMed: 27884713]
43. Prabha S, Sharma B, Labhasetwar V. Inhibition of tumor angiogenesis and growth by nanoparticle-mediated p53 gene therapy in mice. Cancer Gene Ther. 2012; 19:530–7. [PubMed: 22595792]
44. Vasir JK, Labhasetwar V. Biodegradable nanoparticles for cytosolic delivery of therapeutics. Advanced drug delivery reviews. 2007; 59:718–28. [PubMed: 17683826]
45. Gao Z, Zhang L, Hu J, Sun Y. Mesenchymal stem cells: a potential targeted-delivery vehicle for anti-cancer drug, loaded nanoparticles. Nanomedicine : nanotechnology, biology, and medicine. 2013; 9:174–84.
46. Clermont, A., Jenkins, D. Bioware Cell Line LL/2-luc-M38. Caliper Life Sciences, Inc; 2008. p. 1-4.
47. Zhao Q, Ren H, Han Z. Mesenchymal stem cells: Immunomodulatory capability and clinical potential in immune diseases. Journal of Cellular Immunotherapy. 2016; 2:3–20.
48. Chao P, Deshmukh M, Kutscher HL, Gao D, Rajan SS, Hu P, et al. Pulmonary targeting microparticulate camptothecin delivery system: anticancer evaluation in a rat orthotopic lung cancer model. Anticancer Drugs. 2010; 21:65–76. [PubMed: 19966540]
49. Fischer UM, Harting MT, Jimenez F, Monzon-Posadas WO, Xue H, Savitz SI, et al. Pulmonary passage is a major obstacle for intravenous stem cell delivery: the pulmonary first-pass effect. Stem Cells Dev. 2009; 18:683–92. [PubMed: 19099374]
50. Kang SK, Shin IS, Ko MS, Jo JY, Ra JC. Journey of mesenchymal stem cells for homing: strategies to enhance efficacy and safety of stem cell therapy. Stem Cells Int. 2012; 2012:342968. [PubMed: 22754575]
51. Kidd S, Spaeth E, Dembinski JL, Dietrich M, Watson K, Klopp A, et al. Direct evidence of mesenchymal stem cell tropism for tumor and wounding microenvironments using in vivo bioluminescent imaging. Stem cells. 2009; 27:2614–23. [PubMed: 19650040]
52. Wang Q, Cheng H, Peng H, Zhou H, Li PY, Langer R. Non-genetic engineering of cells for drug delivery and cell-based therapy. Advanced drug delivery reviews. 2014

53. Jain RK, Stylianopoulos T. Delivering nanomedicine to solid tumors. Nature reviews Clinical oncology. 2010; 7:653–64.

54. Tredan O, Galmarini CM, Patel K, Tannock IF. Drug resistance and the solid tumor microenvironment. Journal of the National Cancer Institute. 2007; 99:1441–54. [PubMed: 17895480]

55. Fung AS, Jonkman J, Tannock IF. Quantitative immunohistochemistry for evaluating the distribution of Ki67 and other biomarkers in tumor sections and use of the method to study repopulation in xenografts after treatment with paclitaxel. Neoplasia. 2012; 14:324–34. [PubMed: 22577347]

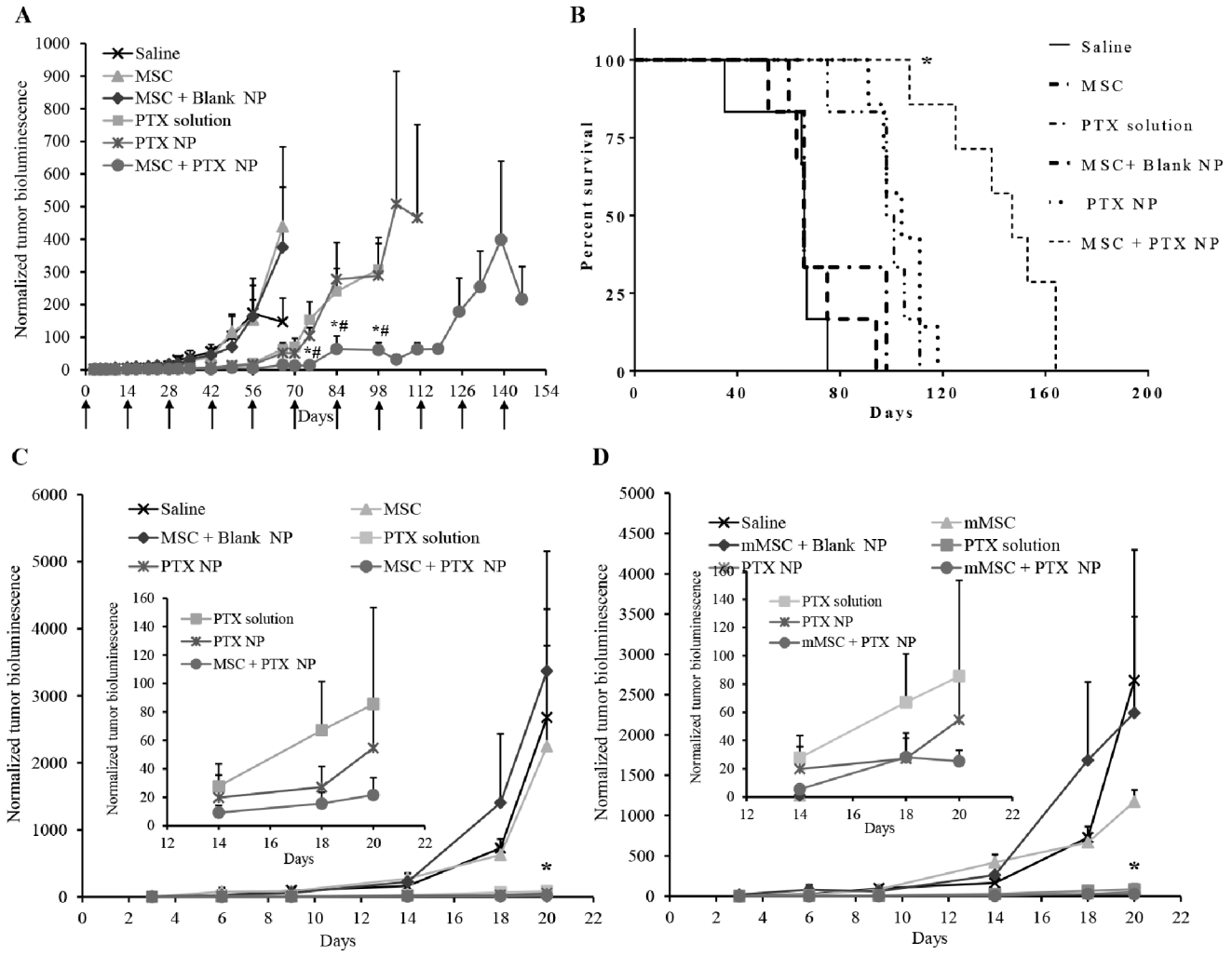

Figure 1. Anti-tumor efficacy of nano-engineered MSCs

(A and B) Mice bearing orthotopic A549 lung tumors were intravenously injected with saline; untreated MSCs (MSC); MSCs engineered with blank nanoparticles (MSC + Blank NP); paclitaxel solution (PTX solution), PTX-loaded nanoparticles (PTX NP); or nano-engineered MSCs (MSC + PTX NP). (A) Plot of normalized bioluminescence readings (± SEM; n=7 for MSC + PTX NP and PTX NP group and n= 6 for all other groups). * significantly different ($P < 0.05$) from PTX solution; # significantly different ($P < 0.05$) from PTX NP. (B) Kaplan–Meier survival curves for the different treatment groups. Log-rank test of MSC + PTX NP and each control group yielded $P < 0.0001$ (*). (C and D) Mice bearing orthotopic Ll/2 lung tumors were intravenously injected with saline; untreated MSCs (MSC); untreated mouse MSCs (mMSC); MSCs engineered with blank nanoparticles (MSC + Blank NP); mouse MSCs engineered with blank nanoparticles (mMSC + Blank NP); paclitaxel solution (PTX solution), PTX-loaded nanoparticles (PTX NP); nano-engineered MSCs (MSC + PTX NP), or nano-engineered mouse MSCs (mMSC + PTX NP). Normalized bioluminescence readings (± SEM; n=7) for (C) human nano-engineered MSCs and (D) mouse nano-engineered MSCs. The insets in C and D show data for PTX solution, PTX NP, MSC + PTX NP, and mMSC + PTX NP on days 14, 18, and 20. For C and D, PTX

solution, PTX NP, MSC + PTX NP, and mMSC + PTX NP are significantly different from non-drug controls ($P < 0.05$)

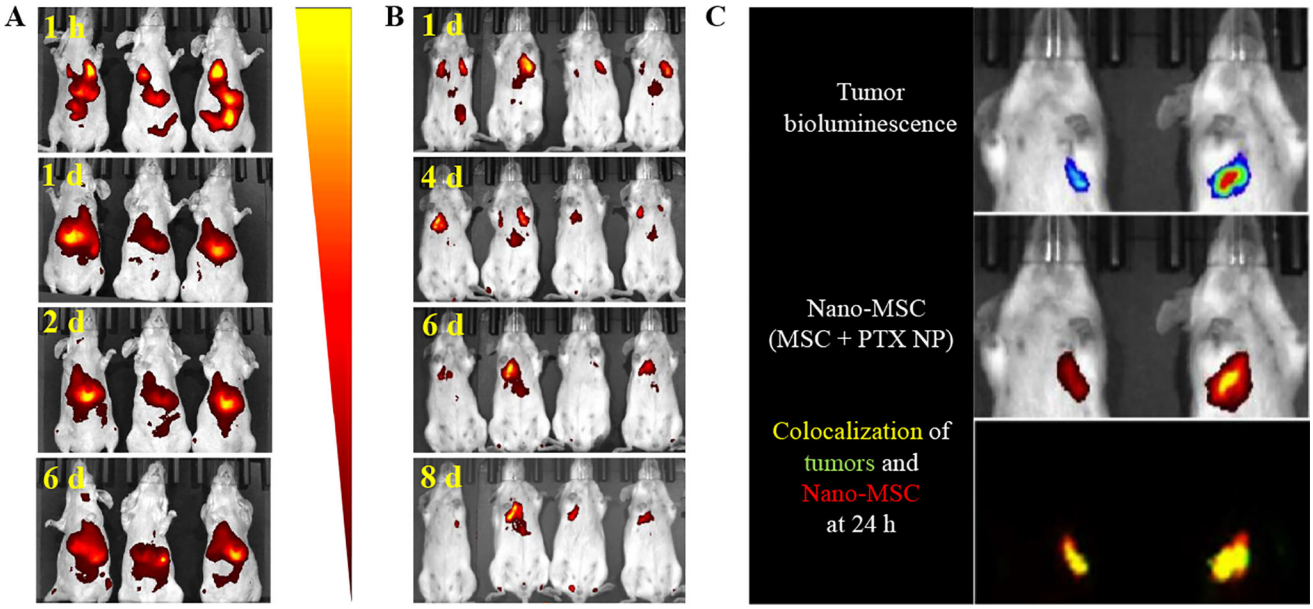

Figure 2. ***In vivo*** **tumoritropic properties of nano–engineered MSCs**

MSCs engineered with near-infrared dye SDB 5491 labeled nanoparticles were injected in both (A) tumor-free and (B) A549–luc orthotopic lung tumor-bearing mice. Fluorescence images were captured at different time points. (C) MSCs engineered with SDB 5491 labeled nanoparticles were injected in A549–luc orthotopic lung tumor bearing mice and both the fluorescence and bioluminescence images were captured at 24 h post injection.

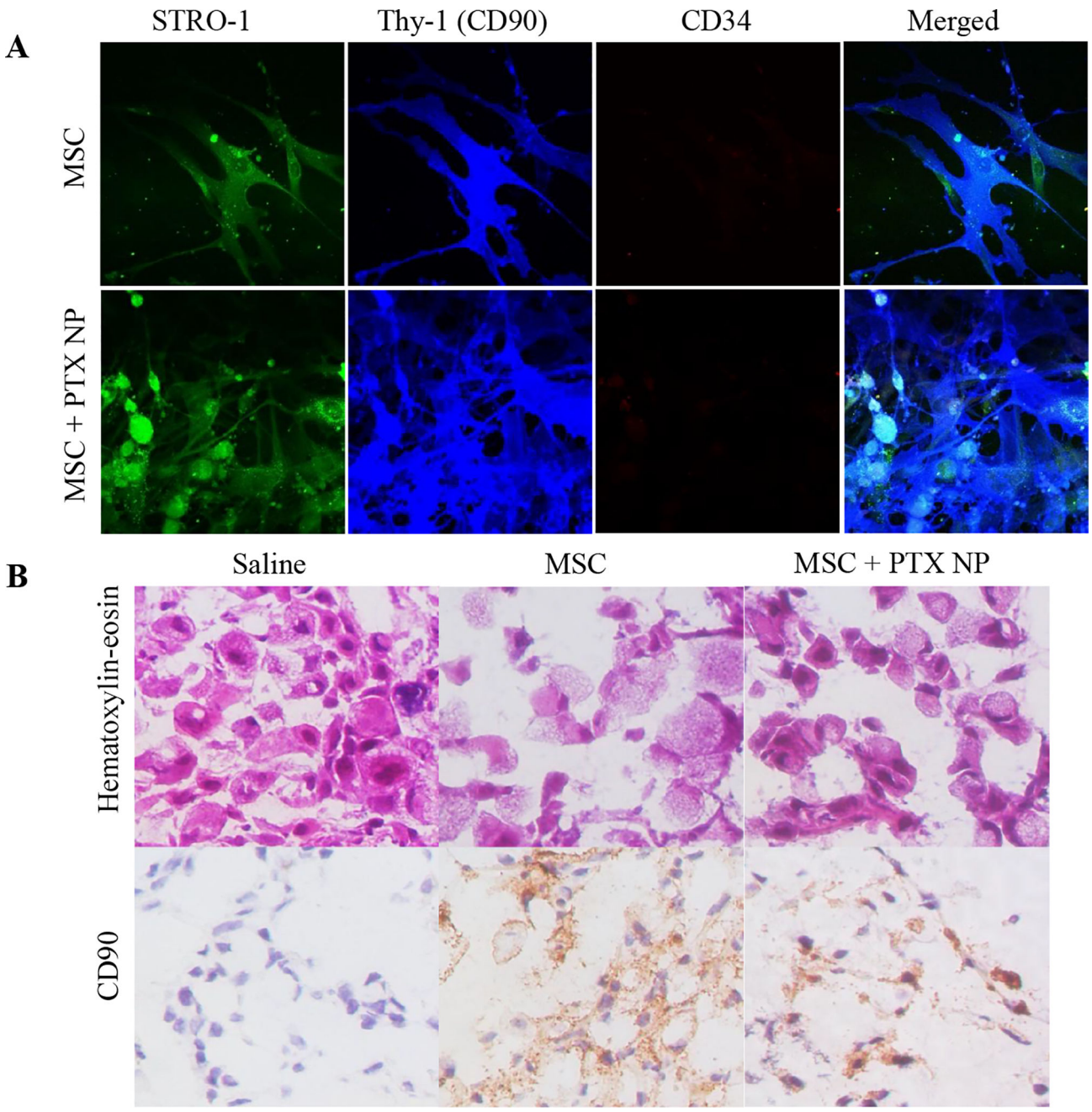

Figure 3.

(A) Effect of nano-engineering on MSC phenotype. Immunofluorescence staining of nano-engineered MSCs. Untreated MSCs were used as controls. MSCs were stained with fluorescently labeled antibodies against specific surface markers such as STRO-1, Thy-1 (CD90), and CD34 antibody. Both untreated MSCs and nano–engineered MSCs had similar staining profile for STRO-1+/Thy-1+/CD 34-. **(B) Intra-tumoral distribution of MSCs.** Tumor tissues from the saline, untreated MSCs, and MSC + PTX NP treated mice were fixed in cold methanol and stained using hematoxylin and eosin and anti-human CD90

antibody followed by DAB staining. Both nano-engineered MSCs and untreated MSCs were found in and around tumor cells. Untreated tissues did not stain for MSCs.

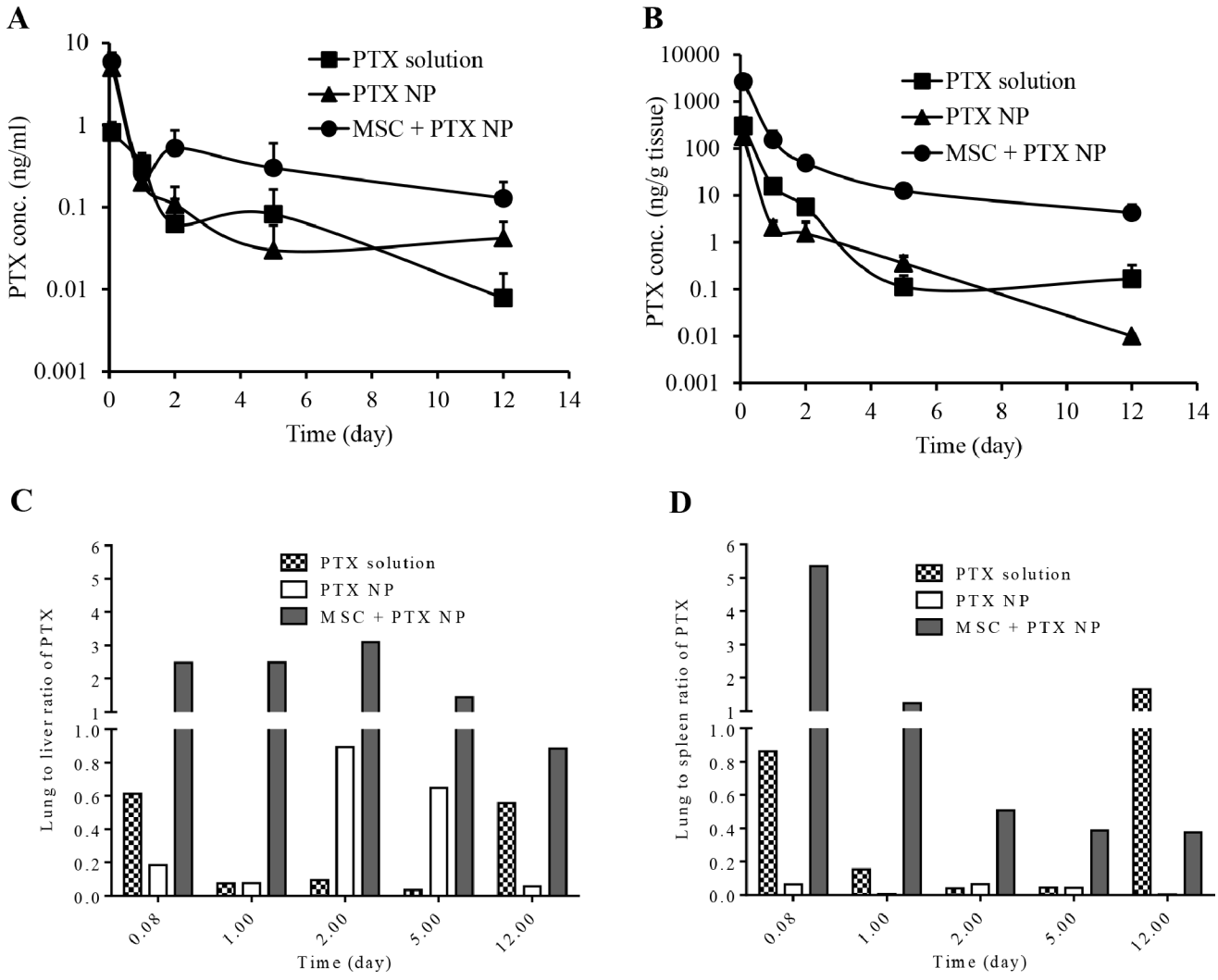

Figure 4. Biodistribution of PTX in tumor-bearing mice

Mice were distributed randomly into 3 groups receiving 5 μg PTX per mouse in the form of solution, PTX-loaded nanoparticles, and nano-engineered MSCs. PTX present in (A) blood, (B) tumor-bearing lungs, and (C) lung to liver ratio and (D) lung to spleen ratio of PTX at different time points were determined. Data represents mean ± SD (n = 3).

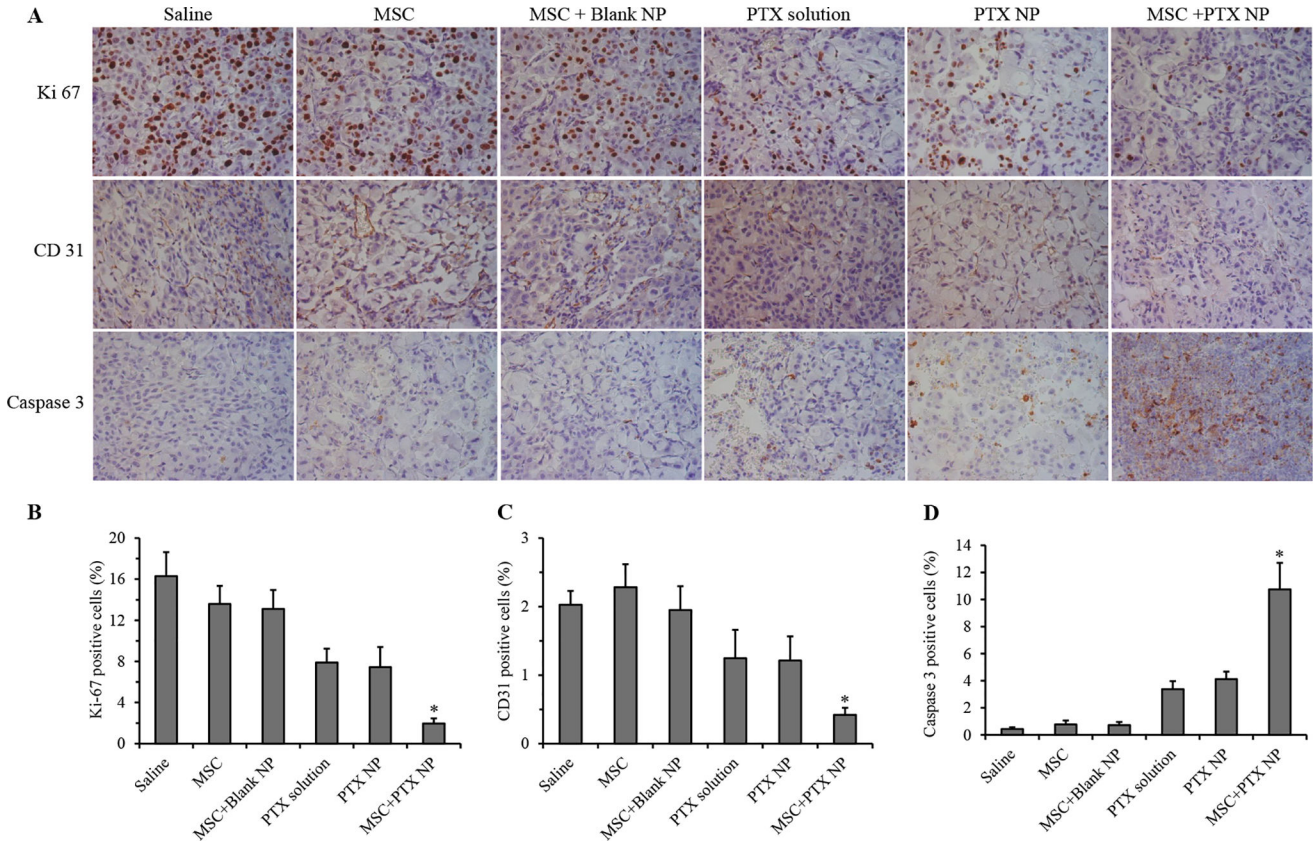

Figure 5. Immunohistological analysis of tumor sections

(A) Tumors were collected at the end of the efficacy study and stained for Ki-67 (for tumor proliferation), CD31 (for angiogenesis), and caspase-3 (for apoptosis). Quantification of (B) Ki67, (C) CD31, and (D) cleaved caspase 3 staining. Data represented as mean ± SD, n = 6 images. * $P < 0.01$ compared to all other treatment groups.

Table 1

Effect of different treatments on complete blood count

Parameters	Saline	MSC + Blank NP	PTX solution	PTX NP	MSC + PTX NP	Normal range
WBC ($\times 10^3$ cells/μL)	9.08 ± 1.29	9.93 ± 1.63	6.73 ± 2.76	5.46 ± 0.57	9.63 ± 1.48	8.69 ± 2.44
RBC ($\times 10^6$ cells/μL)	9.18 ± 0.07	9.72 ± 0.53	7.90 ± 0.33	8.95 ± 0.68	9.95 ± 0.44	9.17 ± 1.05
HGB (g/dL)	14.30 ± 0.34	14.75 ± 0.69	12.23±0.81	13.35±1.33	15.40±0.73	13.72±1.59
PLT ($\times 10^3$ cells/μL)	861 ± 99	767 ± 148	861 ± 146	854 ± 287	759 ± 107	1167 ± 306

WBC: White Blood Cell; RBC: Red Blood Cell; HGB: Hemoglobin concentration; PLT: Platelet count. Data represents mean ± SEM (n = 4)

Table 2

Effect of different treatments on liver function

Parameters	Saline	MSC + Blank NP	PTX solution	PTX NP	MSC + PTX NP	Normal range
ALT (U/L)	21	27	34	32	22	50.53± 37.15
AST (U/L)	75	104	119	66	80	126.54 ± 133.29
GGT (U/L)	1	1	1	1	1	2.59 ± 2.19
ALP (U/L)	233	224	150	149	222	234.51± 93.36
TP (g/dL)	5.0	4.7	4.9	4.9	5.3	5.57 ± 0.95
ALB (g/dL)	3.1	2.9	2.9	2.9	3.3	3.33 ± 0.62
TBIL (mg/dL)	0.21	0.23	0.18	0.21	0.18	0.28± 0.10

ALT: Alanine Aminotransferase; AST: Aspartate Aminotransferase; GGT: γ-(Gamma) Glutamyl Transferase; ALP: Alkaline Phosphatase; TP: Total Protein; ALB: Albumin; TBIL: Total Bilirubin. Blood from four mice was pooled together.